Spring 2008

Modeling Electric Fields in Microfluidic Devices

Micah Fincher

Modeling Electric Fields in Microfluidic Devices

by

Micah Fincher

Undergraduate honors thesis under the direction of

Dr. W Todd Monroe

Department of Biological and Agricultural Engineering

Submitted to the LSU Honors College in partial fulfillment of
the Upper Division Honors Program.

[Spring, 2008]

Louisiana State University
& Agricultural and Mechanical College
Baton Rouge, Louisiana

ACKNOWLEDGEMENTS

Shantanu Kedar, Dr. W Todd Monroe, and Dr. Dimetris Nikitopolous contributed most directly to the success of this project. Kedar is a representative for Coventor Inc. who provided tireless customer service to my many questions. Monroe provided that funds for and access to a private desktop for the sole purpose of working on this thesis. Nikitopolous first introduced me to the Coventor suite and allotted time for me to use his own copy several times a week for the first half of the spring semester.

I would like to additionally thank Julianne Forman Audiffred for her logistical support and biological expertise. I am also indebted to Dr. Jin-Woo Choi and Dr. Chandra Theegala who have served on my committee and have supplied helpful and insightful comments that have greatly improved the quality of my thesis paper and presentation.

-Micah Fincher
Spring 2008

TABLE OF CONTENTS

LIST OF FIGURES

Page No.

ABSTRACT

The miniaturization of components of all types leads to increased portability while reducing material costs. The same is true for medical diagnostic equipment, but often biopsies taken from patients must be transported to a testing facility to perform analyses and evaluations on the samples. With the advent of "lab-on-a-chip" (microfluidic) technologies, such tests are now being incorporated into miniaturized "labs" that are able to perform specific tests for patients at the bedside. Systems that utilize simple electronics for evaluation are generally cheaper and simpler to mass produce. The incorporation of electrodes into simple microfluidic designs may aid in the development of differentiating healthy versus diseased cells. This is important because such a system could be used not only in toxicological testing to help find cures for degenerative diseases, cancer, and AIDS but also for industrial bioreactor culture maintenance and production optimization.

The first step in the design of such systems is software modeling and simulations. Simulations are performed by recreating dimensionally accurate models, assigning appropriate physical properties to the models, and then applying test conditions for analysis. This allows researchers to anticipate and avoid potential problems with a design before wasting time and money on physical fabrication. This thesis uses CoventorWare NetFlow solvers to perform model generation and test analysis to determine how cells will disrupt and concentrate electrical fields created by potentials across embedded electrodes in a microfluidic chip. Discussion of analyses includes various modifications of electrode geometry and cell(s), modeled as a sphere, at differing locations relative to the electrodes.

BACKGROUND

Interest in biologically compatible devices on the micrometer scale has grown rapidly, especially in the last decade. These so-called "microdevices" have blossomed from a nascent group of novel miniaturized devices, originally rooted in silicon-based microfabrication experience, have expanded into more highly developed and integrated "lab-on-a-chip" technologies. The savings in cost and reductions in size that can be expected from such advances is analogous to what has been observed in the computer industry. A common example is that of an everyday blood glucose meter, used by diabetics: the 1969 Ames Diagnostic Glucose Meter was over four inches long, weighed over three pounds, and cost $650 (almost $4000 in 2008 dollars) (1). Today's blood glucose measurements are taken with instruments that could fit in one's pocket and most cost less than $50. Some modern versions are absorbance-based with a light source and photometers, while newer devices are amperometrically based (measuring blood's ability to carry current based on its glucose concentration) (2). This trend toward favoring electronic over optical evaluation is not uncommon because electronic components are easier and cheaper to produce at these scales.

MICROFLUIDICS INCORPORATING ELECTRODES

Just as simple glucose meters have transitioned away from optical detection methods based on transmittance towards electrical recognition, other miniaturized and/or simplified systems are favoring incorporation of electrical detection over optical alternatives. This is most likely due to the high expense of requisite lens and light sensing arrays, which themselves have electronic components for power and information transmission. The replacement of these optical components by mature conductometric, potentiometric, or amperometric methods will expand the possibilities for new simplified tagless (no cell stain) assays.

These technologies are presently being developed concurrently with another trend: miniaturization. The reasoning behind miniaturization is obvious; a reduction in size confers reductions in costs of materials, time to manufacture the product, and transport costs to points of sale. The results of miniaturization abound in everything from cell phones to the width of television sets. Microfluidic devices, containing miniaturized pipes set in plastic with dimensions on the order of millionths of a meter, hold similar promise for diagnostic as well as bed-side applications that minimize sample requirements and experiment times (3). These too are trending toward the incorporation of electronics within them, which is the focus of this thesis.

SIGNIFICANCE & APPLICATIONS OF MODELING

To understand and appreciate the value of modeling microfluidic devices one must first have a general understanding of the time consuming and exhaustive nature of chip fabrication and testing. Figure 1 shows a brief overview of how most of the chips currently in use are fabricated. Each of these four simplified steps have required weeks of optimization and once chips have been fabricated, there is no guarantee that they will be without defects (see pg 18 for a more thorough discussion of the most common chip defects). Modeling helps to circumvent potential problems and to develop expectations for the way electric fields should behave once chips are fabricated. Finding problems while modeling helps to minimize development and fabrication times and material costs.

Coventor, a microfluidics and micro-electro-mechanical systems (MEMS) modeling suite, was chosen as the modeler of choice for all evaluations in this thesis. This robust software has been broadly used

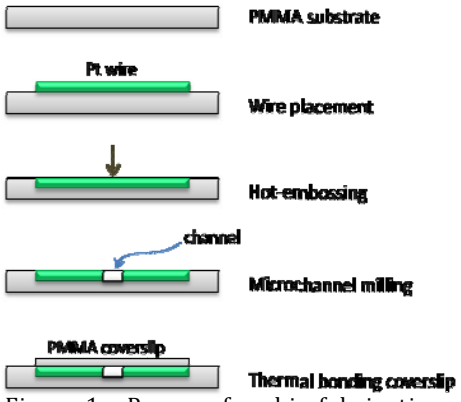

Figure 1 – Process for chip fabrication and wire placement.

for many applications including such varied topics as integrated microfluidics and mixing (4), hydrodynamic focusing (5), and dielectrophoretic sorting (6). Coventor creates 2D and 3D models that can be broken down into finite elements. It then uses a "solver," Netflow in this case, to iteratively solve for values within the model based on initial and/or boundary conditions given. Each example topic above would likely have used the same Coventor modeling, while using different solvers (each has its own functional specialty).

This paper primarily focuses on electrical field propagation through a highly resistive medium between two electrical potentials. How the fields deform when an obstacle is present (such as a cell), is also discussed. Because many other electrokinetic functions are directly dependant on the electrical field magnitude at any given point (such as electrophoresis, dielectrophoresis, and electroosmosis), modeling electric fields is the first step in modeling their potential effects on species or particles in a microfluidic device.

PROCESS AND LAYOUT CREATION

Model creation in Coventor mimics the way lithographic techniques are used to create microsctuctures on silicon wafers. As in lithography, Coventor uses "masks" which "shadow" certain areas on the substrate (see Fig 2) and a protocol (the Process file in Coventor) for adding and removing different materials to and from the substrate. Before the masks can be used, material must be layered on the substrate. This can be done one of three ways: Planar Fill, Stack Material, or Conformal Shell. Fig 2 shows how these different methods behave when applied to the same structure. Once material has been added to a model, it can be further modified by performing additional removal steps using masks from a Layout. Fig 2 simply shows the end result (the model) of the Process file and Layout working together (Fig 3).

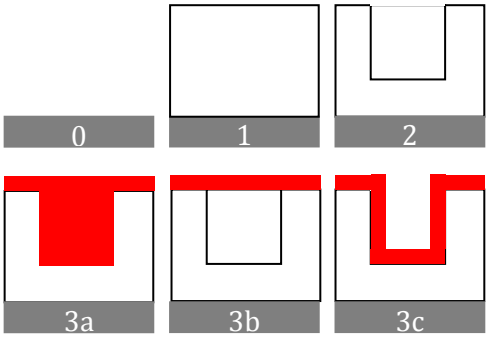

Figure 2 – Side views of: (0) substrate alone, (1) Planar Fill, (2) +resist using mask, (3a) "Planar Fill", (3b) "Stack Material", and (3c) "Conformal Shell".

Each step in the Process must complete before the next step may begin, and performs its function *from above*. Once material has been deposited, the "Straight Cut" action can be used; this function uses a specified layer-mask ("**" in Fig 3, which is simply a square) from the Layout as a positive or negative photoresist. In Fig 2-2 a positive photoresist was used, creating a "⊔" shape. If a negative photoresist was used instead, the model would look like "⊓", with everything removed, *except* for the area shadowed by the layer-mask. Using this method of adding material followed by its selective removal, very complex structures can be constructed. Unfortunately, creating rounded

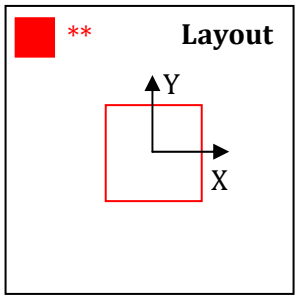

#	Process Step Name	
0	Substrate	null
1	Planar Fill	0.6 in
2	+Straight Cut	0.4 in
3a	Planar Fill	0.1 in
OR		
3b	Stack Material	0.1 in
OR		
3c	Conformal Shell	0.1 in

Figure 3- Layout file and Process used to make models in Fig 2.

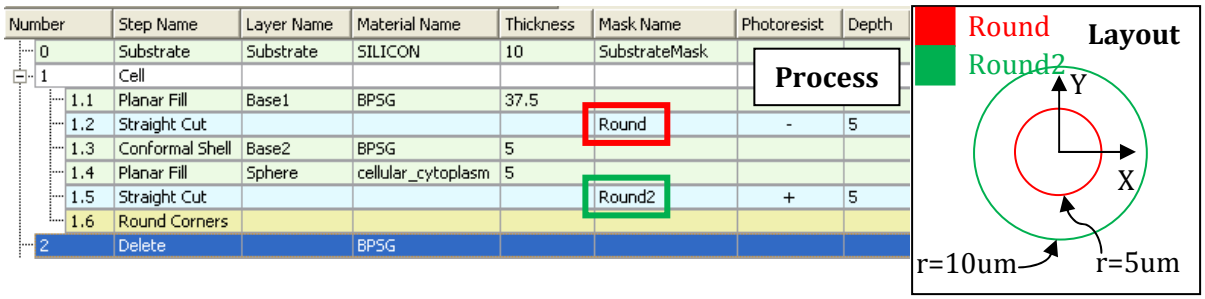

Figure 4 – From left to right: screenshot of Process used to make a sphere and diagram representing Layout with two layer-masks. See Fig 5 for model representations showing how each step contributes to the model.

features in the z-direction (the direction layers are added and cuts are made) is somewhat complex. It is desirable to create such structures, however, because they are more accurate representations of what is physically fabricated.

The following is a short guide showing how a simple model sphere may be created using a Process file and Layout (see Figs 4) to create a model (see Fig 5).

- 0) Substrate – This step, though necessary, is fairly unimportant. If a no layer is designated for it, it will automatically size itself. This layer is often hidden and not part of the final mesh (see next section for more information about meshes).
- Steps 1.1-1.6 are part of what is called a "sequence" – this one is titled "Cell".
- 1.1) Planar Fill – This will add material to fill the entire volume above the substrate. The thickness of this layer will determine the final location of the sphere (the sphere's center will be this step's thickness, plus the length of the sphere's radius – in this case 37.5 +5 =42.5um above the substrate.)
- 1.2) Straight Cut – This is an example of using a *negative photoresist*. It uses the green layer in the Layout ("Round 2", the larger sphere) to remove material added in 1.1.

- 1.3) Conformal Shell – This adds a uniform layer of material to the surface of the material beneath it (see Fig 2-3c). Concave (and convex) corners may be optionally rounded as is shown in Fig 5 (radius of 5um).

- 1.4) Planar Fill – Fill height is measured from the highest point of the layer beneath it. If the fill height is 0, only features below the surface of the previous layer will be filled. This step fills in the bottom half of what will ultimately be the sphere. The material used is 'cellular_cytoplasm', which has default properties automatically associated with it (the cell is modeled as a dielectric).

- 1.5) Straight Cut – This is an example of a *positive photoresist*. This process cuts through the full depth of the previous layer (1.2 was only 5um deep).

- 1.6) Round Corners – This step is analogous to the concave corner rounding feature in 1.3. A radius of 4.9um is used instead of 5 because of erroneous modeling errors sometimes associated with rounding.

- 2) Delete – Base 1 and Base 2 (blue and gold layers above the substrate) were filled with the same material: BPSG (BoroPhosphoSilicate Glass, but any material could have been used). The Delete process is able to delete by material or layer; this time by material – BPSG.

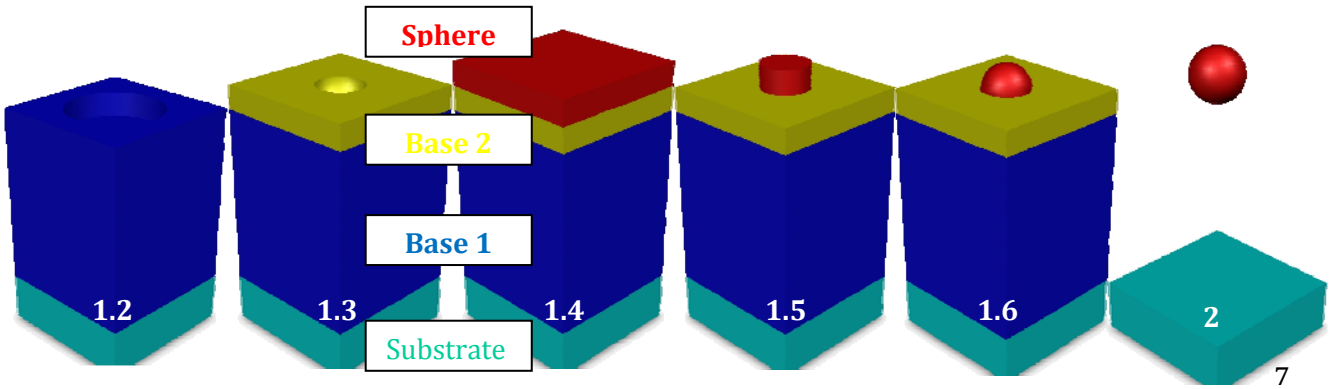

Figure 5- Step-by-step models created from the process and layout shown in Fig 4. Initial Planar Fill step is not shown.

MODEL AND MESH CREATION

Once the sphere has been modeled (remember: its vertical position is based on the thickness of the first Planar Fill step 1.1), additional features can be added using additional Layout layer-masks and Processes. To the bottom right, a model with cylindrical electrodes and buffer added around the original sphere is shown. This model has all the materials necessary for analysis, but is not yet ready for tests. At this phase, the appearance of the model and the material properties of the layers may be modified. For example, the buffer (the translucent, purple rectangular block around the cell in Fig 6) is 80% translucent, and the cell's properties have been changed to be modeled as a dielectric.

Once the model has been created, it should be inspected in the Preprocessor (the program that allows you to view models) to ensure that all layers are appropriately sized and in contact with other layers necessary for the analysis to run correctly. In the model to the right, the anode must be in contact with the cathode to close the circuit applied to them during analyses. Notice the layer-masks in the Layout for the electrodes and the buffer overlap at their interfaces.

Number	Step Name	Thickness	Mask Name
0	Substrate	10	SubstrateMask
1	Cell		
1.1	Planar Fill	37.5	
1.2	Straight Cut		Round
1.3	Conformal Shell	5	
1.4	Planar Fill	5	
1.5	Straight Cut		Round2
1.6	Round Corners		
2	Delete		
3	Electrodes		
3.1	Planar Fill	40	
3.2	Straight Cut		electrode
3.3	Conformal Shell	2.5	
3.4	Planar Fill	0	
3.5	Delete		
3.6	Stack Material	37.5	
3.7	Straight Cut		electrode-top
3.8	Round Corners		
3.9	Straight Cut		electrode-top-cut
4	Planar Fill	2.5	
5	Straight Cut		buffer

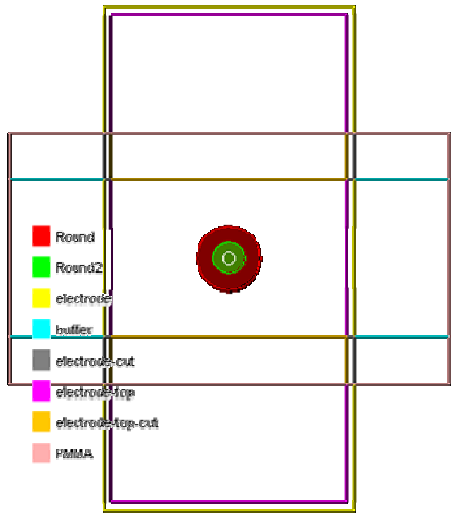

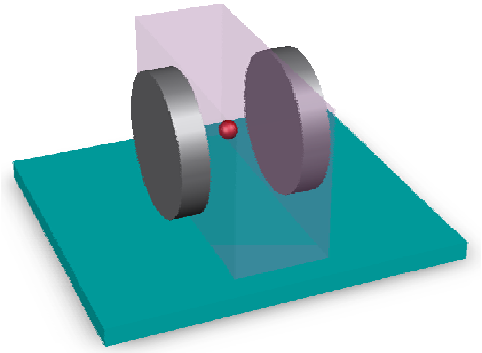

Figure 6 – Process, Layout, and resulting Model used as the basis for most tests. Material used for cylindrical electrodes is Pt. The electrodes are truncated to reduce model size. Buffer is situated between and is contiguous to the electrodes, closing their circuit.

COMPARISON OF MESHER SETTINGS

Figure 7 – Oblique views of three different Mesh Types used on the same model (see Fig 8 below for model and analysis results). From left to right: Manhattan Brick, Tetrahedral, and Extruded Brick types. All have a comparable number of elements – between 58,000 and 64,000.

Meshes may be added to models by right clicking the layers relevant to the desired analysis and clicking 'Add to Mesh Model'. Models with exclusively rectangular features (no rounding) may utilize Manhattan Brick and Extruded Brick mesh types. These are more desirable than the Tetrahedral mesh type because their elements are uniformly smaller, allowing for more refined analyses using fewer elements (and therefore shorter analysis wait times). Notice in Fig 8 the more refined E-field banding in the 'Brick mesh types. "Element size" and "Edge refinement" are additional parameters that greatly affect mesh quality. The Element size determines the maximum length of the edges of the elements created in the mesh. The greater the Element size, the fewer the number elements there will be in the resulting mesh. Edge refinement refers to the concentration of elements ("biasing") at places where different layers meet. This is especially useful when employing Tetrahedral meshing so as to avoid losing refinement of electrical phenomena such as Fringe Effects (E-field concentrations at electrode edges in Fig 8).

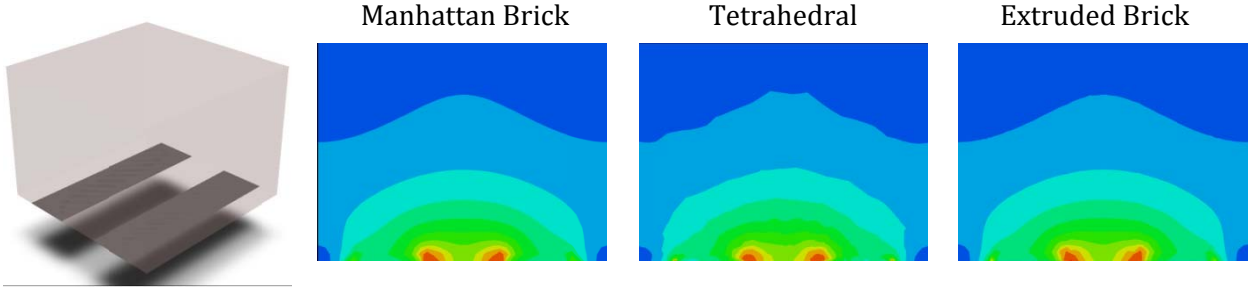

Figure 8 – From left to right: Oblique view of the model used to create meshes in Fig 7, X-Z views of bands of diminishing E-field magnitude (dark blue denotes 0v/cm) on the Manhattan Brick, Tetrahedral, and Extruded Brick mesh types shown in Fig 7 with voltage potential applied across planar electrodes.

MESH FINENESS AND MODEL COMPLEXITY

Just as there are different meshing types, which result in more or less refined results (compare the lines between color bands in Fig 8), the number of "elements," finite volumes the model is broken up into, can also affect the results of a simulation. "Mesh Fineness" refers to the total number of elements of a mesh – the more the "finer." Three meshes generated from the same model are shown in Fig 10, each with progressively greater fineness. Because simulations are regressive computational analyses (that is, the results of initial computations are the inputs for successive computations, and so on), meshes which have few elements may have incomplete or erroneous results. What then makes using as many elements as possible undesirable? As dimensions of elements decrease, their number exponentially increases. As the number of elements increases, the length of time to analyze them exponentially increases. Analyses using highly refined meshes may also become unstable and corrupt. Using Coventor's 'Quality Query' and experimentation with mesh fineness are the best way to find the optimal number of elements for a model.

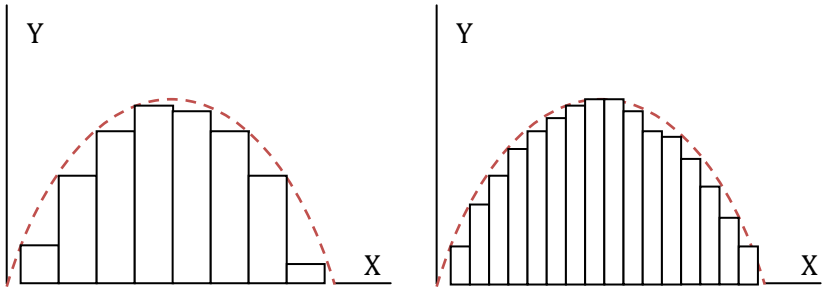

Figure 9- Comparison of meshing to integration. The greater the number of elements, the more accurate the simulation will be. Caveat: meshes with extremely large numbers of elements may create unstable analyses.

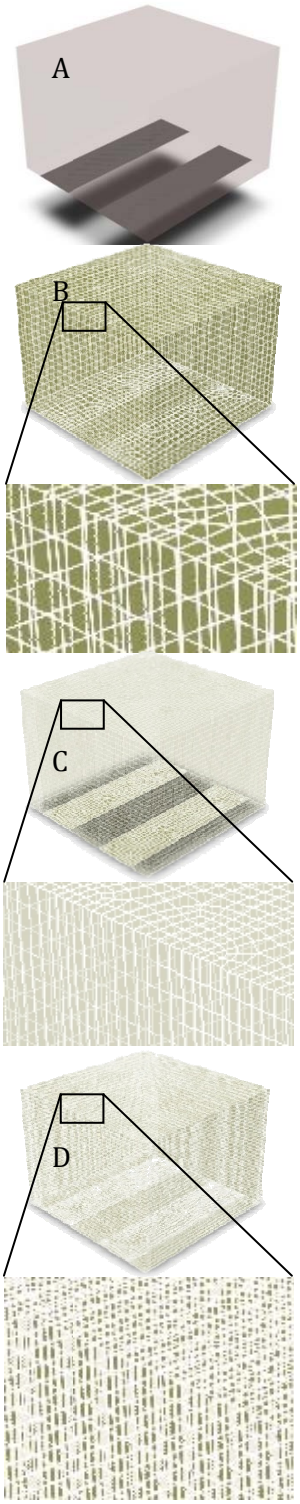

Figure 10 – (A) model, (B) "coarse mesh" with 26k elements, (C) 58k elements, and (D) 122k elements.

ANALYSIS AND VISUALIZATION

Once a mesh has been created for a model, an analyzer can iteratively process the elements based on given boundary conditions. In all analyses in this thesis the boundary conditions have been 10 volts and 0 volts respectively across two parts of the model (and therefore mesh) designated as the "electrodes." The many elements of a mesh can be thought of as a multitude of resistances that serve to close the circuit between the two electrodes.

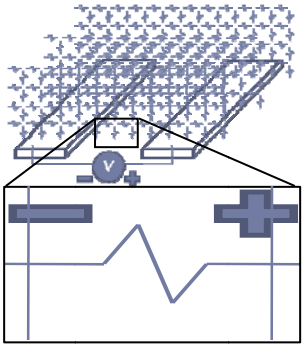

Figure 11 – elements act as numerous resistors acting in parrallel and series. Boundary Conditions (BCs) are given at the "electrodes" – represented by two rectangular shapes here.

Assumptions:

- Steady State → electrodes have been "on" for a while
- Buffer is primary source of resistance → allows for modeling of electrodes only at its buffer interface
- Neglecting temperature effects → heating from e-field is negligible

ANALYSIS BANDING

Analyses will generate colored histograms, areas of similar value, separated by boundary values (see Fig 12). These graphical representations of data are useful for qualitatively comparing differences in electrode geometry or how obstructions in the path of an electric field deform it. To obtain more quantitative data, one must either record the color banding boundaries or directly extract data from an assigned plane (x, y, or z planes, for example). This data can then be plotted and compared to extracted data from other analysis (see Fig 13).

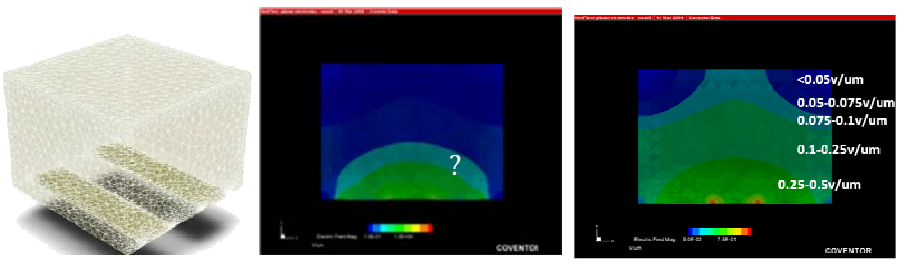

Figure 12 – From right to left: mesh-model, default analysis, and analysis using banding boundaries shown at right. All elements with E-field magnitude >4.5V/um are **red**, those between 1.25- 4.5 V/um are **orange**, etc.

.05
.075
.1
.25
.5
.75
1
1.25
4.5

ELECTRIC FIELD VECTORS & MAGNITUDES

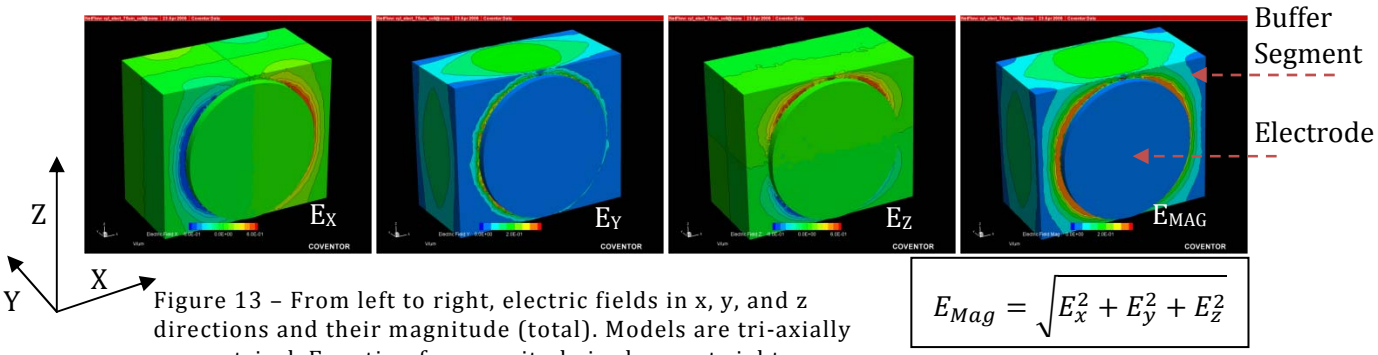

Figure 13 – From left to right, electric fields in x, y, and z directions and their magnitude (total). Models are tri-axially symmetrical. Equation for magnitude is shown at right.

$$E_{Mag} = \sqrt{E_x^2 + E_y^2 + E_z^2}$$

The Coventor Netflow solver computes the electric field produced by the potential across the modeled electrodes in all three dimensions and integrates them into a total magnitude (what is seen in all other analysis figures). In Fig 13, notice that the E_x and E_z fields have positive and negative values (green represents near zero values), each in the positive and negative direction of the plane of those vectors (see axis directions at top-left). The E_y field, which is collinear with the electrodes and the direction of the potential across them, has a significance presence in the modeled buffer.

EVALUATIONS

PLANAR ELECTRODES

As is evident from Fig 14 and 15, the prescence of the cell near planar electrodes (see Fig 12 as a model reference for the analysis without a cell) disrupts and deforms the "quickest path" the electric field tries to take between the two electrodes. As the cell moves away from the electrodes, it disrupts ever weaker electric fields, therefore creating less of a disturbance to the field. Since the

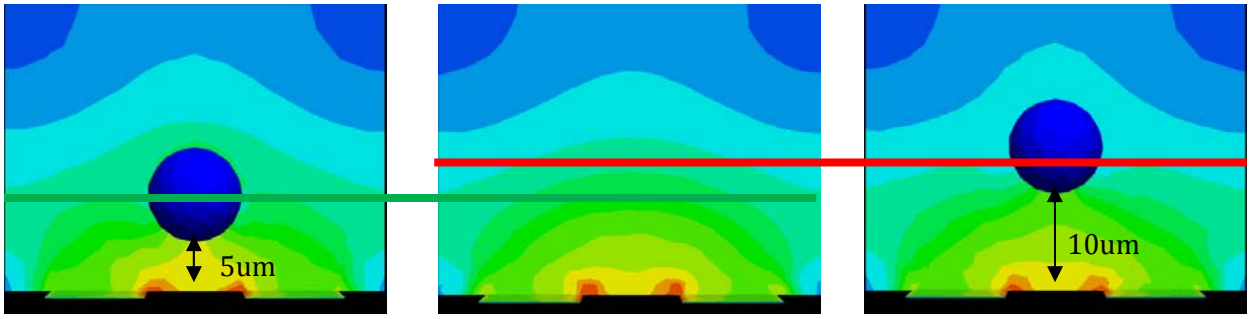

Figure 14 – Differences between presence or absence of a cell and how its distance from the electrode affects the electric field deformations it induces. Electric fields diminish exponentially as a function of distance from the electrodes. See figure 15 for graphical comparison.

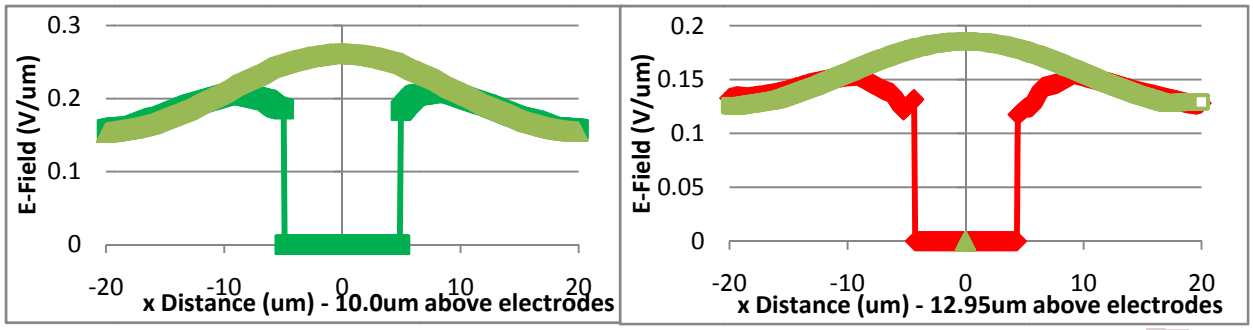

Figure 15 – Graphical representation of the difference between the electrical field with and without a cell present.

electric field decreases exponentially as a function of distance from the electrodes, to obtain the best signals with planar electrodes, the cell should be "rolling" along the channel floor, if possible. This is most conducive to low flow rates and/or tall channels (high aspect ratio).

EVOLUTION OF MODELING

2D MODEL VS 3D SQUARE ELECTRODES

2D models (Fig 16-A) simply do not properly compute the way the electric field deforms around cells, but do provide some basic information about what the expected fringe effects (see Fig 8 for fringe effect example) may be or where the electrical field will likely be weakest within the channel. Because any circular object is treated as a cylinder in 2D models, a 3D alternative (Fig 16-B) that allowed for spherical modeling was necessary.

3D SQUARE ELECTRODES VS 3D CYLINDRICAL ELECTRODES

Square electrodes are useful for identifying the size and intensities of the electric field concentrations and voids around a cell of a given size. They are not as accurate, however, for identifying size and intensities of physically accurate fringe effects. Because the interface the electrodes share with the modeled buffer serves as the basis for

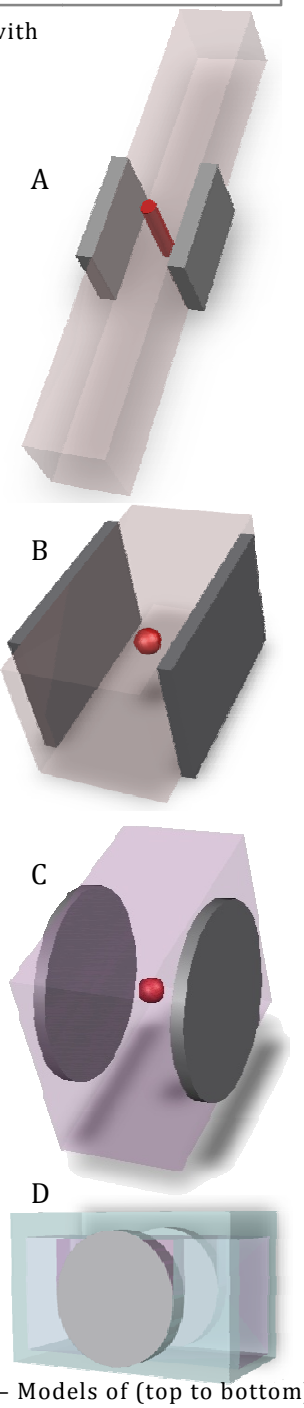

Figure 16– Models of (top to bottom): 2D only 3D with square electrodes, full 3D, and 3D with channels bounded by PMMA

successive elements' values (because analyses are iterative processes), using cylindrical electrodes creates more accurate initial elemental values upon which the buffer's internal elements are dependent.

MODEL COMPLEXITY AND ASSUMPTIONS

With the spherical cell and cylindrical electrodes, what else can be added to make a model (and therefore mesh) more physically accurate? Since the buffer and wire is, in reality, surrounded by PMMA, it would be more physically accurate to incorporate PMMA into the model (see Fig 16-D). However, in doing so, the model becomes larger, thus requiring more elements for the analysis to calculate (resulting in longer analysis time), but the analyses are nearly identical to those that do not incorporate PMMA. This is because PMMA so much less conductive than the buffer or electrodes (see appendix). Thus, it is reasonable to simply leave it out of these tests.

E-FIELD DEFORMATION AS CELL APPROACHES ELECTRODES

As the cell, modeled as a dielectric sphere, approaches the center of the buffer separating the electrodes it is also approaching the area of greatest electric field magnitude (if one is only considering the center of the channel). Because the cell is nonconductive, there are electric field concentrations encircling the cell in the Y plane with spherical voids on either side of the cell in the X and Z planes. As the cell nears the electrodes, thereby displacing greater electric field concentrations, the encircling concentrations and spherical voids grow (Fig 17).

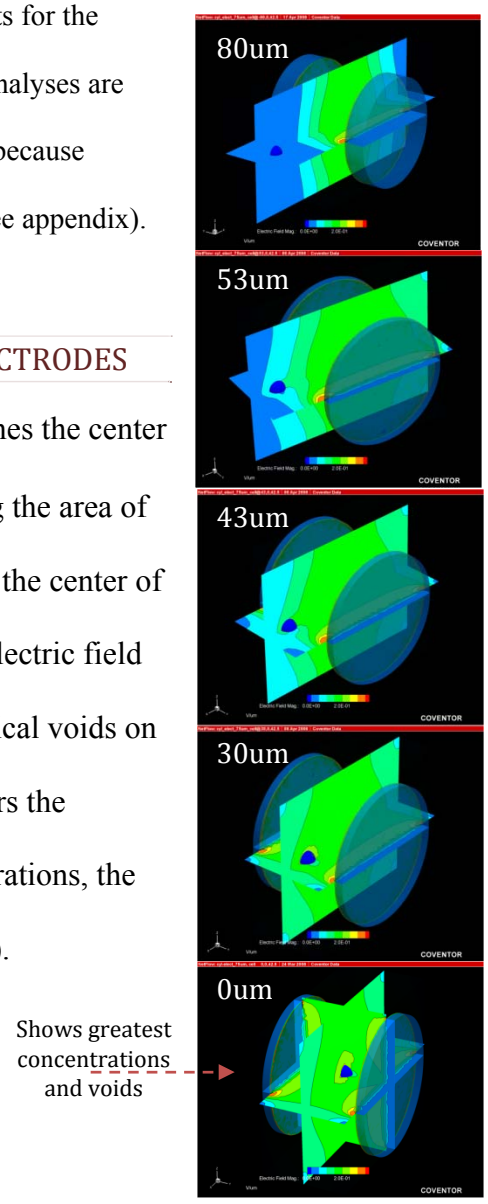

Figure 17 – Distances reported are from the center of the cell to the center of the area separating the electrodes.

VARYING BUFFER CONDUCTIVITY

Fig 18 shows that varying buffer conductivity does not affect electric field formation across the applied 10v. Remember that the field is measured in V/um, so the electrode gap and electrode geometry will have the greatest and most direct effect on electric field formation.

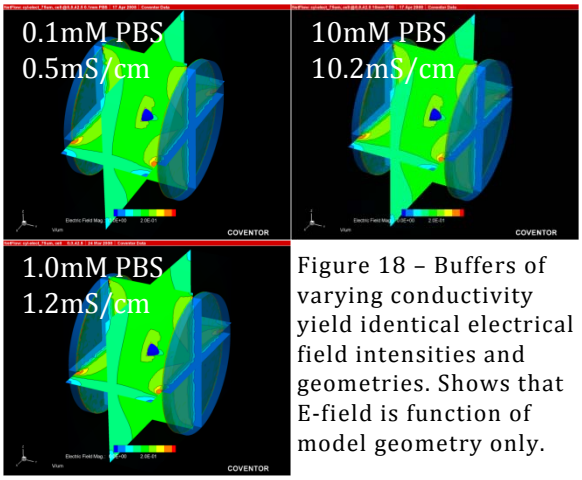

Figure 18 – Buffers of varying conductivity yield identical electrical field intensities and geometries. Shows that E-field is function of model geometry only.

VARYING ELECTRODE SIZE

As electrode size decreases, the electric field concentrations become centered around the electrode-buffer interface in the form of fringe effects (see Fig 19-10um: E-Field spikes are due to this effect). Also, since the gap between the electrodes is large compared to their geometry (50um gap in all cases shown here) the field the cell displaces is relatively weak (the cell's volume is smaller relative to the space separating the electrodes), resulting in a small difference between the cell being present or not. Larger electrodes yield greater electric field concentrations at the center of the buffer separating the

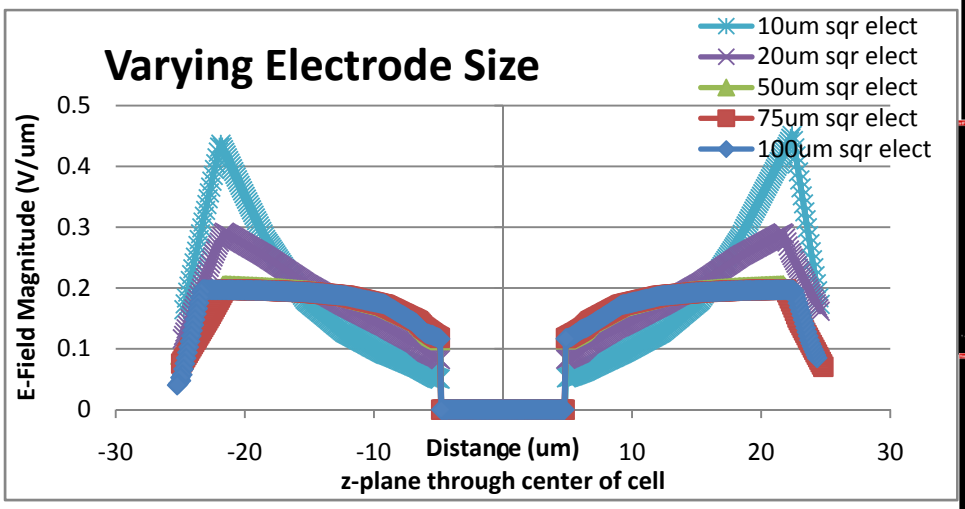

Figure 19 – Values shown are the width and height of square electrodes on either side of a channel. Oblique views are given with slices along all planes through the center of the modeled 10um cell. An enlarged version of this graph is in appendix.

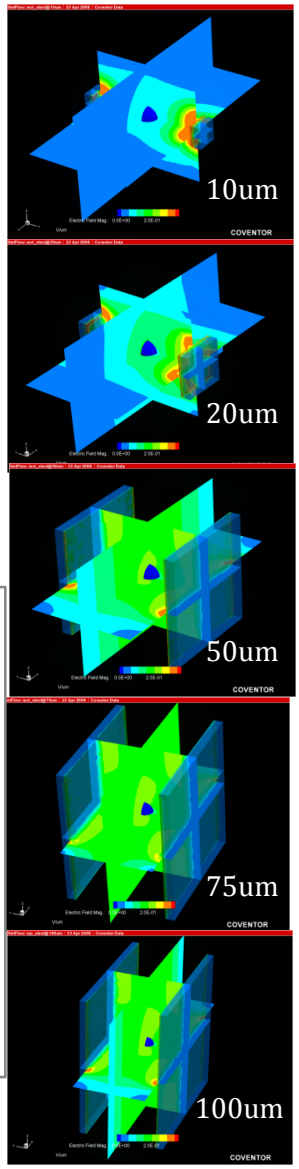

electrodes, thereby maximizing the change in the electric field that the cell affects. This must be balanced, however, with the fact that the cell diplaces only a small portion of the electric field; a portion that decreases relative to larger electrodes or greater electrode gaps. Therefore, the optimal electrode size would appear to be that which was **equal to or less than** the gap between the electrodes. The affect of cell size on these analyses is given on page 17..

VARYING ELECTRODE GAP (∴ MODIFYING CHANNEL GEOMETRY)

If the electric field magnitude is measured in Volts per micron (micrometers), one would imagine that to most drastically alter this value one could either change the voltage potential (the analysis' boundary conditions) or change the gap between the electrodes (change the model itself). Fig 20 shows how merely changing the electrode gap while holding the potential applied at 10v affects not only the electric field, but how the cell interferes with that field. This shows that the optimal channel geometry is that which is narrowest. Of course, this must be balanced with cell velocity and channel clogging considerations.

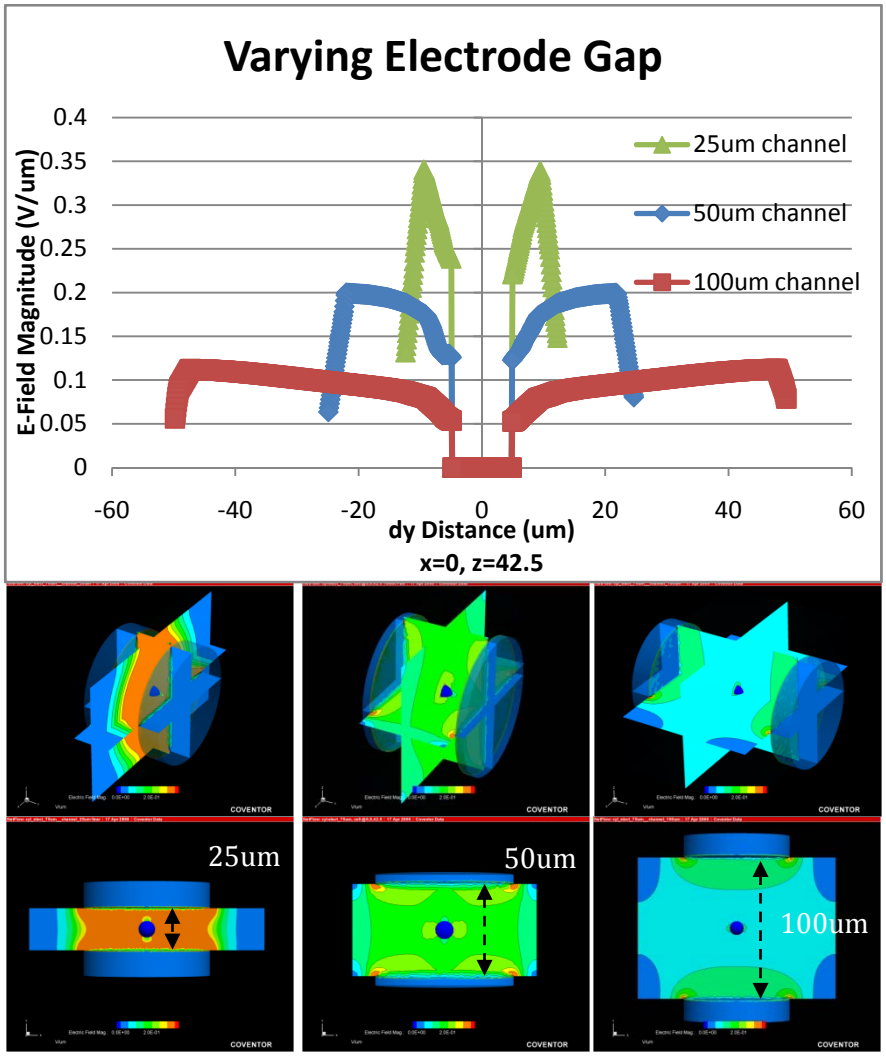

Figure 20 – Graph with oblique and Z-axis (top-down) views shown. Values represent gap distance between cylindrical electrodes. All channels are 80um tall (electrode diameter=75um).

VARYING CELL SIZE

Cell diameter may differ greatly from cell to cell (observed ranges included 8um-12um in diameter for Jurkat cells). This evaluation shows how differences in cell diameter alter the electric field as compared directly to when no cell is present. In each of the most extreme cases (measuring the electric field magnitude down the center of the channel, through the cell itself as graphed in Fig 22), it becomes obvious that larger cells not only create the greatest non-conducting volume (i.e., solely from $V = \frac{4}{3}\pi r^3$) but also from the two voids around the cell (shown by each graph's departure from the "no cell" line at +/- 20um). That the 20um diameter example departs from the "no cell" example the greatest is no surprise, but shows that larger cells (of the same type and viability) will inherently create greater disturbances to the electric field as it passes through it.

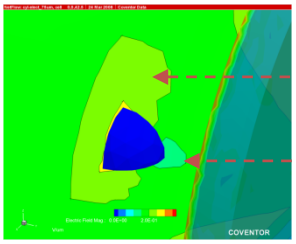

Figure 21- close up view of cell in center of electrodes.

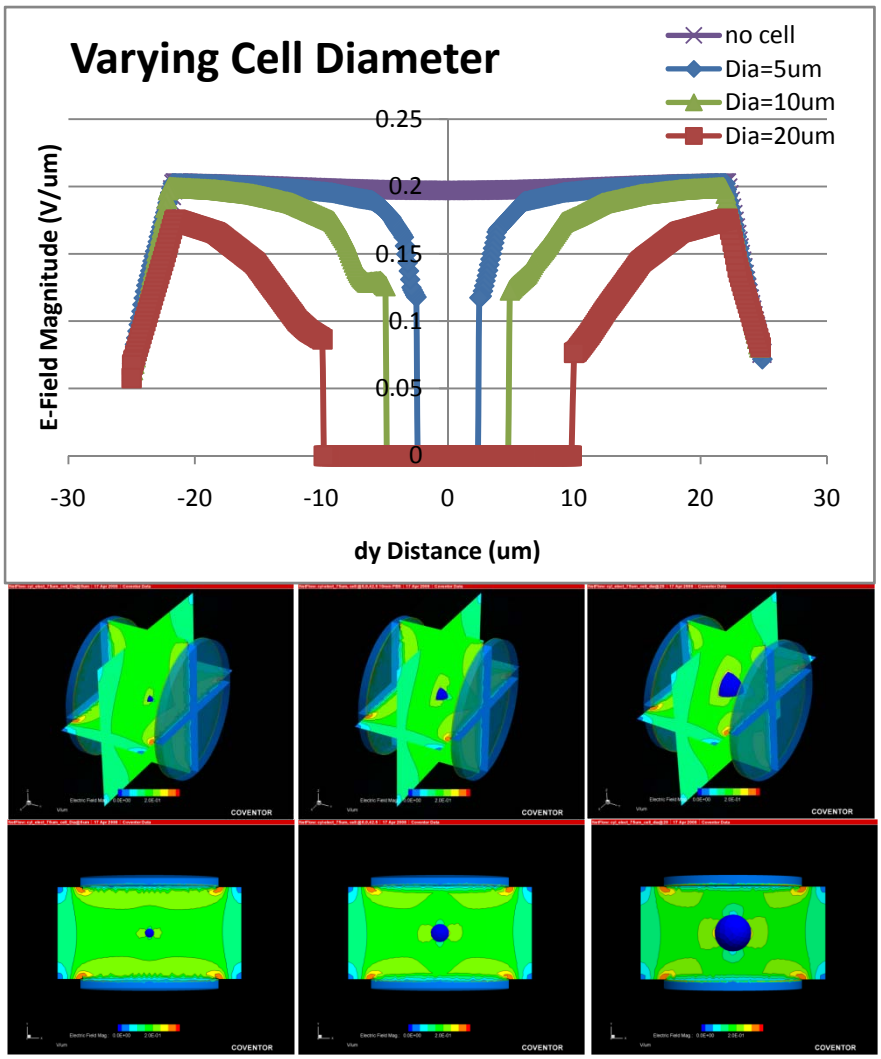

Figure 22 – Graph with oblique and Z-axis (top-down) views are shown. Values given represent cell diameters. Channel gap is 50um with all electrodes at 75um in diameter.

CHIP DEFECTS

Since microchip manufacture is a multi-step procedure (sometimes more "experiment" than procedure, see Fig 1) there may be differences or "defects" in different chip's variation. One of the most common is from the step where the laid wire is micromilled through to create the channel, but a "burr" or small piece of platinum is still connected to the detection wire from a rough cut. Other defects include (especially in chips that have "guide channels", perpendicular to the flow microchannel, in which two wires are laid on either side of the flow channel instead of milling through one wire) protruding or recessed electrodes.

EFFECT OF BURRS

As can be seen in Fig 23, because a burr changes the area of contact between the electrode and the buffer itself, it most drastically alters the local electric field concentrations at that interface. It does not, however, affect the size of electric field concentrations or voids and would likely not interfere with results, so long as the burr's local electric field deformations were not large enough to interfere with those created by the cell (as is the case in Fig 23).

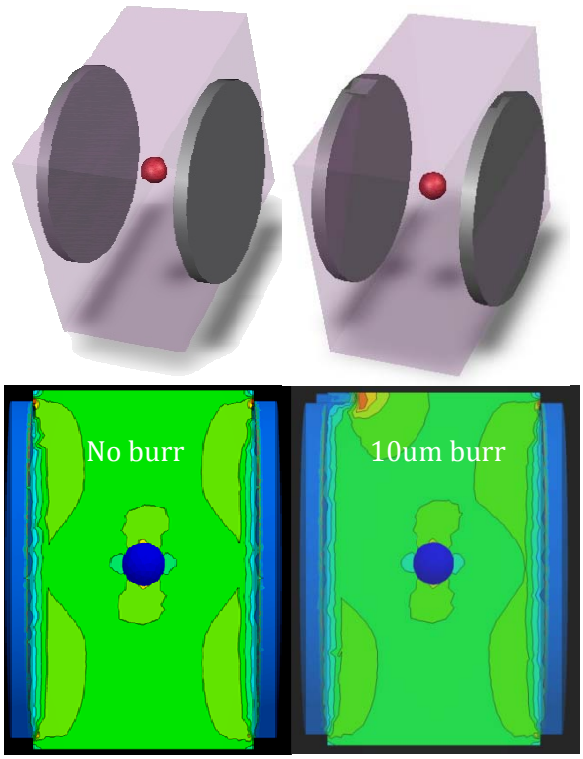

Figure 23 – Model and analysis of the absence and presence of a burr on one of the detection electrodes.

EFFECT OF RECESSED OR PROTRUDING ELECTRODES

Since electrodes gap distance is the greatest determinant of electric field magnitude (see Fig 20) and therefore elicits a greater or lesser change in field deformation as a non-conducting sphere passes through it, recessed or protruding electrodes pose a significant problem because the gap is different from the normal case.

As such, chips with significantly recessed electrodes may get significantly weaker signals from the same cell samples, and chips with protruding electrodes may create clogs or capture cellular debris that may be impossible to remove. Such chips should be discarded.

DISCUSSION

Many models and analyses have been presented, but some discussion remains, such as:

Why is the cell modeled as a dielectric sphere? This is based on the Single-Shell Model (see Fig 24), which is widely used in literature for cell modeling (see (7), (8), and (9) for some recent examples). At low frequency, the cell has high capacitance and the double layer dominates. As the frequency increases, the resistance of internal cellular components begins to contribute to the cell's ability to conduct current. The system for which these models have been created only uses a 40kHz electrical signal to detect cells. At this frequency, neither the cell membrane nor its cytoplasm conducts current through it (>=1MHz would be needed) (10).

What if the discounting of temperature effects is inapplicable to these cases? Transient changes to the chip's buffer temperature would likely increase the buffer's resistance to current flow. Changes in buffer resistance, however, do not change the shape or magnitude of the electric field (see Fig 18).

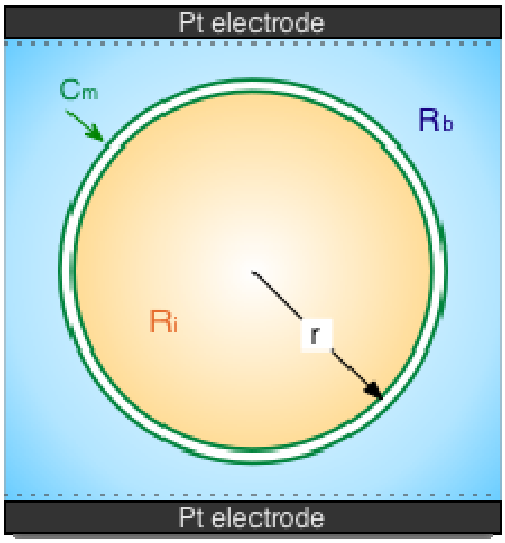

Figure 24 – Cm= Cell membrane capacitance, Rb= resistance of buffer, and Ri is resistance of cytoplasm. Cf. Julianne Forman Audiffred.

Why has 10V been chosen as the potential across the electrodes? This is a figure used in initial evaluations which was continued to be applied for the

sake of consistency. Because the electric field magnitude is directly proportional to the voltage applied (doubling the potential will double the electric field magnitudes in all areas of the evaluation), any voltage could have been used for these comparison evaluations. In reality, there are merely picovolts applied at the electrodes in the real chips. Evaluation values can simply be divided by 10V and multiplied by the actual applied voltage to find what the expected values would be in other applications.

FUTURE WORK

Topics include:

- Verification of alternating current detection modeling has similitude with direct current evaluations
- Combining electrophoretic or dielectrophoretic modeling with detection electrodes
- Exploring other Coventor solvers to model spherical movement in response to applied potentials
- Use of dielectrophoretic modeling for cell sorting

CONCLUSIONS

Coventor Neflow modeling and solvers are powerful tools that aid researchers in microfabrication design execution and in developing quantitative expectations for how the electric fields in their devices are distributed. Modeling recommendations include creating meshes fine enough to effectively capture details that may be lost from inefficient meshing, especially in the vacinity of interfaces of the electrodes and buffer.Also it is worth noting that 2D models are less effective than 3D square electrodes, which are inferior to 3D cylindrical

electrodes.These models yield comparable results relative to more “physically accurate” models incorporating PMMA to bound the cell buffer and electrodes.

Planar electrodes are useful if techniques are employed to localize the cell near the electrodes, or for flow rates low enough to allow cells to “roll” on the bottom of the microchannel.For higher throughput applications, side wall electrodes (SWEs) may be perferrable. When designing microfluidics incorporating SWEs, one should note that the greatest detection will be from the largest cells (assuming cells differ only in size) directly between the electrodes. Minimizing the gap between SWEs and avoiding electrodes diameters greater than their gap will also help maximize detection. When evaluating fabricated chips, one must more readily reject chips with protuding or recessed electrodes as they may give significantly different results relative to other chips. They may have to be calibrated individually. Chips with burrs, however, may be acceptable as long as cells are measured in a consistant place relative to the electrodes.

SUMMARY BIBLIOGRAPHY

1. **Sattley, Melissa.** The History of Diabetes. *Diabetes Health.* [Online] November 1, 1996. http://www.diabeteshealth.com/read/1996/11/01/715.html.

2. *Planar Amperometric Glucose Sensor Based on Glucose Oxidase Immobilized by Chitosan Film on Prussian Blue Layer.* **Jianzhong Zhu, Ziqiang Zhu, Zongsheng Lai, Rong Wang, Xiaoming Guo, Xiaqin Wu, Guoxiong Zhang, Zongrang Zhang, Yiting Wang, Zongyou Chen.** 2002, Sensors, Vol. 2, pp. 127-136.

3. *Disposable Smart Lab on a Chip for Point-of-Care Clinical Diagnostics.* **Chong H. Ahn, Jin-Woo Choi, Gregory Beaucage, Joseph H. Nevin, Jeong-Bong Lee, Aniruddha Puntambekar, And Jae Y. Lee.** 1, 2004, PROCEEDINGS OF THE IEEE, Vol. 92.

4. *Towards numerical prototyping of labs-on-chip: modeling for integrated microfluidic devices.* **Erickson, David.** 2005, Microfluid Nanofluid, Vol. 1, pp. 301-318.

5. *Three-dimensional hydrodynamic focusing in polydimethylsiloxane (PDMS) microchannels.* **Sundararajan N, Pio MS, Lee LP, Berlin A.** 2004, MEMS, Vol. 13, pp. 559-567.

6. *Micro total analysis systems: Recent developments.* **Vilkner T, Janasek D, Manz A.** 2004, Anal Chem, Vol. 76, pp. 3373-3385.

7. *Effects of T-tubules on dielectric spectra of skeletal muscle simulated by boundary element method with two-dimensional models.* **Sekine K, Hibino C , Kimura M , Asami K.** 2, 2007, Bioelectrochemistry, Vol. 70, pp. 532-541.

8. *Dielectric spectroscopy of single cells: time domain analysis using Maxwell's mixture equation.* **Sun T, Gawad S , Green NG , Morgan H.** 1, 2007, JOURNAL OF PHYSICS D-APPLIED PHYSICS, Vol. 40, pp. 1-8.

9. *Effects of membrane disruption on dielectric properties of biological cells.* **Asami, K.** 21, 2006, JOURNAL OF PHYSICS D-APPLIED PHYSICS, Vol. 39, pp. 4656-4663.

10. *Impedance spectroscopy flow cytometry: On-chip label-free cell differentiation .* **Cheung K, Gawad S, Renaud P.** 2, 2005, CYTOMETRY PART A , Vol. 65A, pp. 124-132.

APPENDIX

Material	Use	Conductivity
"Cellular_Cytoplasm"	Cell - Sphere	1E3 pS/um or dielectric
"PBSbuffer"	Buffer for cell and to close circuit created by electrodes	0.1mM = 5.0E4 pS/um 1.0mM = 1.2E5 pS/um 10.0mM = 1.02E6 pS/um
"Platinum"	Electrodes	9.66E12 pS/um
"PMMA"	Chip volume containing buffer	0.0 pS/um

Boundary Conditions: 10vdc and 0vdc at external faces of left/right or top/bottom electrodes.

Color Banding for all analyzer figures (unless otherwise specified): 0, 0.05, 0.1, 0.15, 0.2, 0.25, 0.3,< max>
-note: figures in the Electric Field Vectors and Magnitudes have +/- bands of the above set.